energies

MDPI

Article

Experimental Investigation of Flow Boiling Heat Transfer in an Annular Minichannel with ZnO-, ZnO/PMHS-, and Al_2O_3-Modified Heated Surfaces

Magdalena Piasecka [1,*], Krzysztof Galiszewski [1], Artur Piasecki [2], Monika Maziukienė [3], Raminta Skvorčinskienė [4], Ainė Antanavičė [4] and Simas Račkauskas [5]

1 Faculty of Mechatronics and Mechanical Engineering, Kielce University of Technology, 25-314 Kielce, Poland; kgaliszewski@tu.kielce.pl
2 Faculty of Environmental Engineering, Geomatics and Renewable Energy, Kielce University of Technology, 25-314 Kielce, Poland; apiasecki@tu.kielce.pl
3 Department of Energy, Kaunas University of Technology, Studentu Street 56, LT-51424 Kaunas, Lithuania; monika.maziukiene@ktu.lt
4 Laboratory of Combustion Processes, Lithuanian Energy Institute, Breslaujos Street 3, LT-44403 Kaunas, Lithuania; raminta.skvorcinskiene@lei.lt (R.S.); aine.antanavice@lei.lt (A.A.)
5 Institute of Materials Science, Kaunas University of Technology, K. Barsausko St. 59, LT-51423 Kaunas, Lithuania; simas.rackauskas@ktu.lt
* Correspondence: tmpmj@tu.kielce.pl

Abstract

Subcooled flow boiling of distilled water was investigated in a vertical annular minichannel with smooth and surface-modified heated tubes. Copper and stainless-steel substrates were tested with ZnO and ZnO/PMHS coatings; Al_2O_3 was additionally tested on stainless steel. A simplified one-dimensional cylindrical model provided local effective heat transfer coefficients, and modified surfaces were compared pointwise with smooth references at matched operating conditions and axial positions. A modification was considered favourable only when the heat transfer coefficient increased without an increase in wall temperature. ZnO on stainless steel was the only modification meeting this criterion at both nominal mass flow rates: the mean pointwise coefficient increased by 44.2% at 7 kg/h and 42.9% at 10 kg/h, while mean wall temperature decreased by 36.9 and 32.8 K, respectively. Al_2O_3 and ZnO/PMHS on stainless steel reduced the coefficient and increased wall temperature, whereas copper modifications showed no robust improvement relative to the designated references. A separate model-sensitivity assessment did not alter the qualitative ranking. ZnO-modified stainless steel was therefore the best-performing configuration within the tested matrix; no broader superiority is claimed beyond the present geometry, fluid, flow rates, and heat-flux range.

Keywords: flow boiling; annular minichannel; heat transfer coefficient; ZnO coating; ZnO/PMHS; Al_2O_3 coating; distilled water

Academic Editor: Jan Taler

Received: 17 July 2026
Revised: 21 August 2026
Accepted: 25 August 2026
Published: 26 August 2026

1. Introduction

Flow boiling in mini- and microchannels is an established method for removing high heat fluxes from compact thermal systems [1]. Reducing hydraulic diameter increases the surface-to-volume ratio but also makes the response strongly dependent on surface condition, local vapour generation, pressure drop, and liquid replenishment. In annular minichannels, wall curvature and the narrow annular gap additionally affect bubble growth, local liquid-film distribution, and thermal-boundary-layer development [2–5].

Surface modification is a direct approach to altering boiling heat transfer [1,6–8]. Modified surfaces can change the onset of nucleate boiling, active nucleation-site density, bubble departure, rewetting, critical heat flux, and wall-temperature stability. The effect is not universal: a surface that promotes nucleation may also increase vapour retention, while a strongly wettable surface may improve liquid supply without providing sufficient nucleation activity. The resulting response depends on the coupled effects of wettability, roughness, morphology, coating stability, substrate material, and flow conditions.

Hydrophilic and superhydrophilic surfaces generally favour liquid spreading and rewetting, whereas hydrophobic domains can lower the barrier for vapour embryo formation [6–9]. Either tendency can become unfavourable if it respectively suppresses nucleation or promotes excessive vapour retention. Static wettability should therefore be treated as one surface descriptor rather than as a stand-alone predictor of flow boiling performance.

Mixed-wettability surfaces illustrate this competition particularly clearly: hydrophobic regions can promote nucleation, whereas hydrophilic regions support liquid replenishment [6,8]. Most demonstrations concern pool boiling or selected microchannels; transfer to an annular minichannel is nontrivial because the confined annular gap imposes different constraints on liquid and vapour transport.

The present study investigates subcooled flow boiling of distilled water in an annular minichannel. Coatings play an important role in heat transfer processes and can significantly influence the thermal behaviour of the surface. Three modifications with different coating chemistries and measured wetting states were considered: ZnO, ZnO/PMHS, and Al_2O_3. ZnO provides a structured oxide surface, ZnO/PMHS introduces a lower-surface-energy modification while retaining the ZnO framework, and Al_2O_3 provides a chemically different ceramic-oxide surface. The comparison therefore tests whether coating chemistry or static wettability alone can predict thermal performance, or whether the coating–substrate combination must be considered jointly. The selected coatings can be applied by immersion-based procedures and are compatible with cylindrical substrates. Smooth reference surfaces and the three classes of modification were compared using a corrected cylindrical data-reduction model. The primary indicators were the local heat transfer coefficient, wall temperature, and axial heat transfer profiles obtained during increasing and decreasing heat flux.

Modified surfaces were compared pointwise with the corresponding smooth reference of the same substrate at matched nominal heat-flux levels and axial positions, with the increasing- and decreasing-heat-flux branches treated separately. This differential approach reduces the influence of baseline variability on the surface ranking; the full matching protocol is given in Section 5.2.

A modification was classified as favourable only when the local heat transfer coefficient increased without an accompanying increase in wall temperature. This rule is study-specific, not a universal definition of boiling enhancement, and is justified in Section 5.2.

The objective of this work was to determine which tested coating–substrate combinations provided a thermal advantage over their smooth references under matched subcooled flow boiling conditions. The main contribution is a pointwise comparative assessment across two substrates using local heat transfer coefficient and wall temperature as complementary performance indicators.

2. Literature Background

A comprehensive review by Liang and Mudawar [1] shows that channel flow boiling enhancement by surface modification can improve heat transfer coefficient and critical heat flux, but it can also increase pressure drop or introduce flow instabilities. This is important for minichannel design, where enhancement must be assessed using thermal, hydraulic and repeatability criteria rather than by the maximum coefficient only.

Betz et al. [6] demonstrated that the best pool-boiling performance is not necessarily obtained on uniformly superhydrophilic or uniformly superhydrophobic surfaces. Biphilic surfaces combining hydrophilic and hydrophobic regions can manage liquid and vapour transport more effectively. Although that work concerned pool boiling, the underlying requirement for simultaneous nucleation promotion and rewetting is directly relevant to confined flow boiling.

Phan et al. [7] investigated flow boiling of water on nanocoated surfaces in a single rectangular microchannel and showed that wettability strongly affects the heat transfer coefficient. Ahmadi et al. [8] examined gradient mixed-wettability surfaces in a high-aspect-ratio microchannel; compared with a fully hydrophobic reference, the biphilic surfaces produced heat transfer enhancement of up to 56.7%, while flow visualisation showed a reduction in the bubbly flow regime and extension of the slug flow regime. These studies demonstrate that wettability patterning can alter both thermal performance and two-phase flow structure, but they also underline that results obtained in planar microchannels cannot be transferred directly to a confined annular geometry.

Wciślik et al. [10] examined static contact-angle determination for TiO_2-water nanofluids using controlled sessile-drop dosing and several profile-fitting approaches. Both the dosing conditions and the fitting model affected the measured value: differences between geometric fits and the Young–Laplace method reached approximately 10–15°, while the coefficient of variation was about 2–5% for Young–Laplace fitting and 8–12% for the geometric approaches. These findings justify treating the static contact angle in the present study as a protocol-dependent surface descriptor rather than as an absolute material constant.

Kaniowski and Wciślik [11] measured contact angle and surface tension for deionised water, ethanol, Novec-649 and FC-72 on copper surfaces and analysed their role in nucleate pool boiling, including bubble departure modelling. The study illustrates that wettability-related quantities depend on both the working fluid and the surface condition. This is directly relevant to the present interpretation because water-based wetting trends should not be transferred uncritically to refrigerants or dielectric liquids.

Surface-processing studies provide additional methodological context. Radek et al. [12] showed that laser treatment of electro-spark-deposited WC-Co coatings altered surface roughness and microstructure while improving coating adhesion and corrosion resistance. Orman et al. [13] directly linked laser-generated microfins and roughness to pool-boiling performance: for the tested geometries, surfaces with 0.4 mm microfins dissipated more than three times the heat flux of surfaces with 0.2 mm microfins for water and about twice as much for ethanol, with the strongest benefit at low wall superheat. Żórawski et al. [14] showed that the composition and processing parameters of plasma-sprayed Al_2O_3–$3TiO_2/CaF_2$ coatings affected roughness, hardness and friction. These studies are not direct annular-flow comparators, but they illustrate how coating deposition and post-processing can modify several surface attributes simultaneously.

Annular and mini-annular channels require geometry-specific interpretation. Lu and Wang [15] experimentally studied single-phase water flow in a narrow annulus and found an earlier transition from laminar to turbulent heat transfer than in conventional circular tubes. At Reynolds numbers below 150, axial heat conduction had an important influence on the overall thermal response, and the two data-processing approaches considered in that study gave particularly different results below Reynolds numbers of about 400. More recently, Yang et al. [16] combined experiments and computational fluid dynamics for a horizontal mini-annular water channel with a 3.0 mm gap; within the investigated Reynolds-number range of 1100–1729, the flow behaved turbulently, and the Nusselt number increased with Reynolds number, heat flux and inlet temperature. Together, these results support the use of a data-reduction procedure consistent with the actual annular geometry rather than direct transfer of conventional-tube assumptions.

Studies of coating-controlled wetting and vapour-layer behaviour provide useful context for the ZnO-based surfaces, although they concern regimes different from the present subcooled flow boiling. Maziukienė et al. [17] showed that TiO_2-containing coated surfaces and surrounding-water temperature affected cooling dynamics and Leidenfrost vapour-film formation. Vorotinskienė et al. [18] investigated a superhydrophobic Al–ZnO+PDMS coating containing ZnO tetrapods and polydimethylsiloxane (PDMS). Because that study concerned Leidenfrost vapour-film behaviour rather than subcooled flow boiling and used PDMS instead of the PMHS modification employed here, it is treated as mechanistic context rather than as a direct material analogue. The review by Mardosaitė et al. [9] further showed that ZnO wettability depends on nanoscale morphology, crystallographic orientation and oxygen-related surface defects, with Wenzel- and Cassie–Baxter-type states and reversible wettability changes possible under environmental or thermal stimuli. Accordingly, ZnO is treated here as a structured oxide, ZnO/PMHS as a lower-surface-energy variant retaining the ZnO framework, and Al_2O_3 as a chemically different ceramic oxide; no single wettability descriptor is assumed to predict boiling performance.

Hożejowska and Piasecka [19] used a two-dimensional Trefftz formulation to determine local heat transfer coefficients during HFE-649 flow boiling in a 2 mm annular minigap and reported pronounced axial variation. The present study uses a different data-reduction approach, based on a simplified radial-conduction correction adapted to the coaxial heated element.

Annular gap flow boiling depends on coupled geometric and operating parameters [2,3]. Boye et al. [2] showed interacting effects of gap width, heat flux, mass flux, inlet temperature and vapour quality in 0.5–1.5 mm annuli. Chen et al. [3] found higher R-407C boiling coefficients in a 1 mm than a 2 mm annular gap and linked changes in heat flux and subcooling with bubble departure, frequency and active nucleation-site density. These results show why local axial changes cannot be attributed to surface properties alone.

The importance of the surface structure itself was demonstrated in earlier HFE-649 experiments in a 1 mm annular minigap [4]. Five mechanically or electrochemically enhanced surfaces were compared with a smooth copper surface. The surface produced by spark erosion yielded the highest local heat transfer coefficients in the saturated-boiling region, whereas one of the threaded surfaces produced coefficients lower even than those obtained for the smooth surface. The enhancement therefore depended on the type of surface structure and was not a universal consequence of increasing roughness or geometric development. The same study also showed that the local coefficient generally decreased downstream in both the subcooled and saturated boiling regions.

Flow resistance and heat transfer were jointly investigated in a separate study [5] using HFE-649 in a different annular-minigap experimental module with different instrumentation and data acquisition. That study showed that hydraulic performance requires separate evaluation. Consequently, its pressure-drop results are not quantitatively compared with those obtained in the present experiments. The present study focuses exclusively on the thermal performance of the coated surfaces in the current distilled-water annular minichannel.

Despite these studies, direct comparative data for ZnO-, polymer-functionalised ZnO-, and Al_2O_3-modified surfaces tested on different metallic substrates under the same annular-minichannel flow boiling conditions remain limited. In particular, it remains unclear whether nominal wettability or coating chemistry alone can predict a favourable thermal response, or whether the coating–substrate combination and the local boiling conditions must be considered jointly. The present study addresses this gap using matched local comparisons with the corresponding smooth substrates.

3. Materials and Methods

3.1. Experimental Facility and Annular-Minichannel Geometry

The experimental setup consisted of a closed-loop circulation system, an annular-minichannel test module, a heating and power-supply system, and a data-acquisition system. A schematic diagram of the experimental rig is shown in Figure 1a, whereas Figure 1b presents a photograph of part of the laboratory stand, including the test-section assembly. Distilled water was used as the working fluid. The flow was generated by a Tuthill gear pump, and the mass flow rate was measured using an Endress+Hauser Promass A Coriolis flowmeter (Endress+Hauser Flowtec AG, 4153 Reinach BL, Switzerland). Heating power was supplied to a cartridge heater mounted inside the inner cylindrical element of the test section and controlled by a programmable GW Instek ACR-2100 power supply (Good Will Instrument Co., Ltd., New Taipei City, Taiwan).

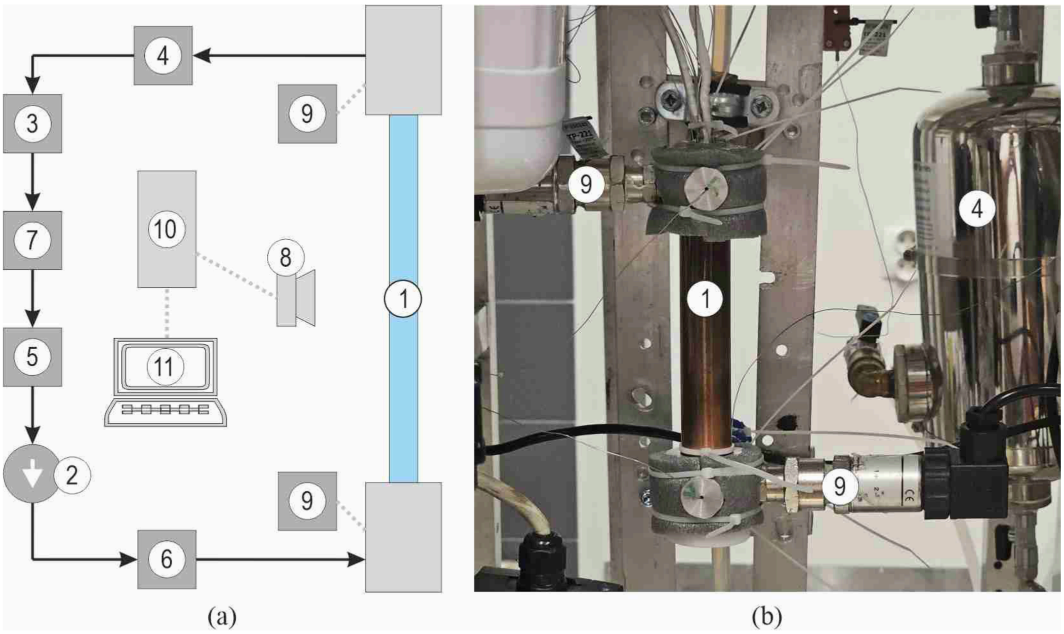

Figure 1. Experimental rig: (**a**) schematic diagram of the closed-loop circulation system; (**b**) photograph of the test-section assembly, including the annular-minichannel module and adjacent components of the experimental setup; 1—test section with an annular minichannel; 2—circulating pump; 3—compensating tank; 4—condenser; 5—filter; 6—Coriolis mass flow metre; 7—deaerator; 8—high-speed camera; 9—pressure transducers; 10—data acquisition station; 11—computer.

The annular minichannel was formed between the outer surface of an interchangeable heated metal tube and the inner surface of a coaxial borosilicate glass tube. The test-module geometry is presented in Figure 2a,b. Figure 2a shows the longitudinal schematic view with the axial positions of the thermocouples located in the heater-tube interspace. Figure 2b presents the cross-sectional schematic view of the annular-minichannel geometry, including the coaxial arrangement of the cartridge heater, heated metal tube and outer-glass tube. Figure 2c shows a photograph of the test module assembly. Fluid temperature and overpressure were measured at the inlet and outlet of the test section, while electrical parameters, temperature, pressure and flow rate were recorded using the data-acquisition system. The essential specifications of the experimental setup are listed in Table 1. The 1 s sampling interval enabled monitoring of the approach to steady conditions and averaging of the stabilised part of each measurement series.

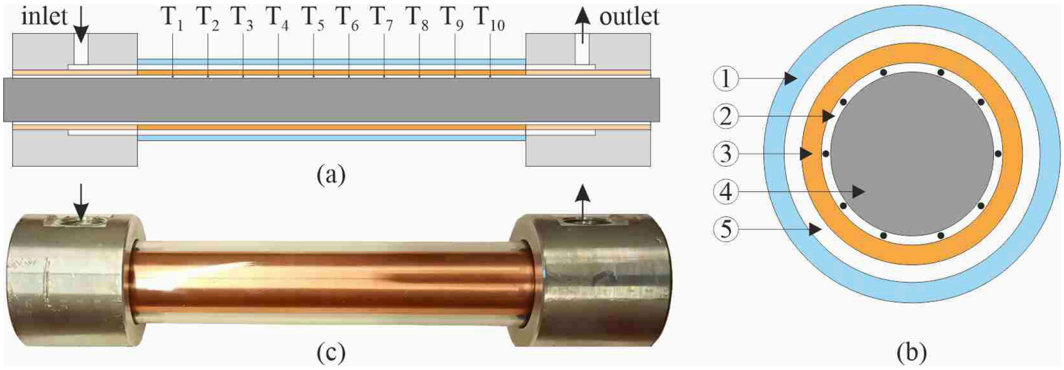

Figure 2. Annular-minichannel test module: (**a**) longitudinal schematic view showing the axial positions of the thermocouples located in the heater-tube interspace; (**b**) cross-sectional schematic view of the annular-minichannel geometry; (**c**) photograph of the test module assembly. 1—glass tube; 2—heater-tube interspace, locally accommodating the thermocouples; 3—interchangeable heated metal tube with the tested surface modification; 4—cartridge heater; 5—annular minichannel.

Table 1. Main parameters of the annular-minichannel experimental setup.

Description/Value	Parameter
Distilled water	Working fluid
Annular gap between coaxial cylindrical surfaces	Minichannel geometry
15.0 mm	Cartridge-heater diameter
7.5 mm	Assumed thermocouple radius in the simplified mathematical model
18.0 mm	Outer diameter of heated metal tube
20.4 mm	Inner diameter of glass tube
1.2 mm	Minigap width
110 mm	Active minichannel length
0.0024 m	Hydraulic diameter
Borosilicate glass tube; optical access to the flow	Outer wall
Copper: 398 W/(m·K); stainless steel: 15.1 W/(m·K); grade-consistent sensitivity assessed in Section 5.3	Substrate thermal conductivity used in the main data reduction
Tuthill gear pump (Tuthill Pump Group, Alsip, IL, USA)	Circulation in the flow loop
Endress+Hauser Promass A Coriolis flowmeter	Flow measurement
T-type thermocouples at the minigap inlet and outlet, Czaki Thermo-Product (CZAKI Thermo-Product Sp. z o.o., Raszyn-Rybie, Poland)	Fluid temperature measurement
WIKA S-10 pressure transducers at the minichannel test module inlet and outlet (WIKA Alexander Wiegand SE & Co. KG, Klingenberg, Germany)	Overpressure measurement
WIKA A-10 absolute pressure transmitter (WIKA Alexander Wiegand SE & Co. KG, Klingenberg, Germany)	Atmospheric pressure measurement
Graphtec GL840 data logger (Graphtec Corporation, Yokohama, Japan)	Data acquisition
GW Instek ACR-2100	Power supply

The wall-temperature instrumentation consisted of ten 0.5 mm-diameter T-type thermocouples seated in grooves machined in the cylindrical surface of the cartridge heater. The grooves were approximately 0.5–1.0 mm deep. The first junction was positioned 10 mm from the beginning of the analysed section; successive junctions were spaced at 10 mm axial intervals and rotated circumferentially by 36°. The thermocouples were maintained in direct contact with the heater and point-fixed with a high-temperature adhesive. The junction-centre radius was estimated to be 7.0 ± 0.25 mm. The cartridge heater was closely fitted inside the metal tube with an inner diameter of 15 mm. In the one-dimensional model, 7.5 mm was adopted as the effective radial coordinate corresponding to the inner radius of the tube rather than the exact radial position of the thermocouple junctions. The implications of this modelling assumption are discussed separately in Section 5.3.

3.2. Tested Surfaces and Coating Preparation

The heated surface was prepared using interchangeable cylindrical tubes. The stainless-steel substrate was identified as 0H18N9/EN 1.4301/AISI 304, and the copper substrate as Cu-DHP/CW024A/2.0090, temper R290. The manufacturers of the original tubes are unknown. The copper matrix comprised smooth, ZnO, and ZnO/PMHS surfaces. The steel matrix comprised smooth, ZnO, ZnO/PMHS, and Al_2O_3 surfaces. The Al_2O_3 coating was thermally tested only on the steel substrate in the present experimental matrix, although a copper + Al_2O_3 specimen was included in the surface-characterisation set. The thickness of the dip-coated layers was estimated to be approximately 10–30 µm based on the coating procedure, observed hierarchical morphology, and surface roughness measurements. For each substrate and nominal mass flow rate, the corresponding smooth tube was used as the differential reference. The tested thermal matrix is summarised in Table 2, and representative surface views are shown in Figure 3. This range is a descriptive estimate based on the deposition procedure, the observed hierarchical morphology, and the measured surface roughness; it was not obtained from direct cross-sectional thickness measurements and should not be interpreted as an experimentally measured minimum-to-maximum interval.

Table 2. Tested substrate-surface matrix and coating codes used in the thermal experiments.

Role in the Present Thermal Matrix	Coating Code	Surface State	Substrate
Reference surface for the copper series	-	Smooth	Copper
ZnO-modified copper surface	A	ZnO	Copper
Low-surface-energy ZnO/PMHS-modified copper surface	C	ZnO/PMHS	Copper
Reference surface for the steel series	-	Smooth	Stainless steel
ZnO-modified steel surface	A	ZnO	Stainless steel
Low-surface-energy ZnO/PMHS-modified steel surface	C	ZnO/PMHS	Stainless steel
Ceramic-oxide coating tested thermally only on steel	B	Al_2O_3	Stainless steel

Preparation of ZnO coating (coating A). Polished samples were first immersed in a TEOS solution prepared by mixing 66 mL of isopropanol with 10 mL of tetraethyl orthosilicate (TEOS). Separately, 20 mL of isopropanol and 3 mL of acidified deionised water (pH 3–4, adjusted with HCl) were mixed and then slowly added to the TEOS solution under continuous stirring. The resulting solution was stirred for an additional 15–30 min. The samples were immersed in the prepared TEOS solution for approximately 30 s and then left to dry. Subsequently, the samples were immersed in a ZnO suspension prepared by dispersing 2 g of ZnO tetrapods in 100 mL of isopropanol, followed by sonication for 15–30 min. The ZnO tetrapods were produced by combustion synthesis following the procedure described previously [20]. The ZnO powder consisted of nanoscale tetrapod structures; the tetrapod arms were approximately 300–1000 nm long and approximately

20–100 nm in diameter. Finally, the coated samples were heated at 100 °C for 1 h to promote crosslinking and stabilise the ZnO coating structure.

Figure 3. Representative views of the tested modified surfaces: ZnO and ZnO/PMHS coatings on copper and stainless-steel substrates, and the Al_2O_3 coating on the steel substrate.

Preparation of Al_2O_3 coating (coating B). The preparation procedure was identical to that described for the ZnO coating. The only modification was the replacement of ZnO tetrapods with Al_2O_3 particles in the coating suspension. All subsequent processing steps, including TEOS pretreatment, particle deposition, drying, and thermal treatment, were carried out under the same conditions as those used for the ZnO coating, resulting in the formation of an Al_2O_3 coating structure.

Preparation of ZnO/PMHS coating (coating C). The coating procedure was identical to that described for the ZnO coating until completion of the ZnO deposition and drying steps. The samples were then additionally immersed for 30 s in a 0.5 vol.% PMHS solution, followed by heat treatment at 100 °C for 1 h. The additional PMHS treatment produced a lower-surface-energy ZnO/PMHS coating.

The ZnO, ZnO/PMHS, and Al_2O_3 coatings were not modelled as separate conductive layers because coating thickness and effective thermal conductivity were not measured specimen-by-specimen. Porosity and adhesion were likewise not quantified. Their influence is therefore represented through the experimentally determined effective substrate–coating–fluid heat transfer response. For the model-sensitivity assessment, the coating contribution is varied directly through an area-specific thermal resistance R''_c rather than by assigning unsupported specimen-specific conductivity values. In particular, the effective thermal conductivity, porosity, and adhesion of the present coatings were not experimentally quantified.

3.3. Surface-Characterisation Methods

Surface roughness was characterised using a contact profilometer operating in stylus mode. Profile measurements were conducted over a 3000 μm scan length with a lateral resolution of approximately 1 μm. A stylus with a tip radius of 12.5 μm and a loading force of 3 mg was employed, while each scan required approximately 10 s. The average roughness parameter R_a was calculated from the recorded surface profiles. For each specimen, measurements were repeated at three independent positions, and the roughness values are reported as mean values with standard deviations where available.

Water contact-angle measurements were performed before and after the flow boiling experiments. Static contact-angle values were used as surface descriptors. Because advancing and receding contact angles were not available for the present set, contact-angle hysteresis could not be evaluated.

After the thermal experiments, the coated tubes were cut open and mechanically flattened for post-test contact-angle measurements. Consequently, they could not be reinstalled in the test module. Repeatability was therefore assessed using independent smooth copper runs from the original experimental campaign. Future campaigns will include repeat boiling runs before post-test surface characterisation.

The surface morphology of the coatings was characterised using a Hitachi S-3400N scanning electron microscope (SEM, Hitachi, Tokyo, Japan). SEM images were acquired at an accelerating voltage of 10 kV and a magnification of 5000×. Image analysis was performed with ImageJ software 1.54p. SEM was used to document surface topography and morphology before and after the experiments and to support subsequent interpretation of differences in the thermal response. The images represent the inspected locations only; they are not used to claim quantitative axial or circumferential uniformity of the coating over the complete cylindrical surface.

3.4. Experimental Procedure

Before each experimental series, the flow loop was filled with distilled water and deaerated. After the required mass flow rate had been set, the system was allowed to reach stable hydraulic and thermal conditions. Heater power was then changed through discrete stepwise settings, first increasing to the maximum programmed value and subsequently decreasing. No continuous heating or cooling rate was prescribed. Each operating point was held until the measured temperatures, pressure, and flow rate were sufficiently stable for averaging.

Temperature, pressure, mass flow rate and heater-power data were recorded at 1 s intervals. The present data reduction used averaged values from the stabilised interval of each operating point. The increasing- and decreasing-heat-flux branches were retained separately for the pointwise comparison. Each operating point was treated as an individual steady experimental state; no interpolation between consecutive heat-flux settings was introduced.

No external heat-loss correction was applied in the present analysis because the outer glass-wall temperature was not measured during the water experiments. Consequently, the electrical heater power was used as the nominal heat input in the data-reduction model. In future experimental campaigns, the outer glass-wall temperature should be measured so that an external heat-loss term can be included in the energy balance without double-counting the heat transferred from the heater to the fluid.

4. Data-Reduction Model and Heat Transfer Coefficient Determination

A simplified local one-dimensional cylindrical-wall model was used to reconstruct the fluid-side wall temperature and the local heat transfer coefficient. The formulation follows the concentric-layer concept used previously for annular-minigap heat transfer analysis [19], but the present reduction was restricted to radial conduction through the metal tube at each thermocouple position.

The electrical power P was assumed to pass radially through the metal tube of active length L, with a uniform axial distribution of heat input over L. The thermocouple temperature $T_{TC}(z)$ was referred to the effective model radius r_{TC} = 7.5 mm, while the wall-fluid interface was located at r_w = 9.0 mm. For consistency with the historical data reduction, the retained substrate thermal-conductivity values were 398 W/(m·K) for copper and 15.1 W/(m·K) for stainless steel. The original bibliographic source of these legacy constants could not be recovered; their influence was therefore checked separately against grade-consistent reference values in the model-sensitivity assessment (Section 5.3).

The fluid-side wall temperature was calculated from:

$$T_w(z) = T_{TC}(z) - \frac{P}{2\pi\, k_s\, L} ln\left(\frac{r_w}{r_{TC}}\right) \tag{1}$$

where T_w is the local wall temperature (°C or K), T_{TC} is the thermocouple temperature (°C or K), P is the electrical heater power (W), k_s is the substrate thermal conductivity [W/(m·K)], L is the active heated length (m), r_w is the outer tube radius (m), r_{TC} is the effective thermocouple radius (m), and z is the axial coordinate (m). Equation (1) assumes steady, one-dimensional radial conduction through the metal tube and uniform axial distribution of P over L. Writing the correction in terms of total electrical power avoids ambiguity between heat fluxes referred to the inner and outer cylindrical surfaces.

The heat flux at the outer metal surface and the local heat transfer coefficient were calculated as:

$$q''_w = \frac{P}{(2\pi\, r_w\, L)} \tag{2}$$

$$\alpha(z) = \frac{q''_w}{T_w(z) - T_{f,ref}(z)} \tag{3}$$

where q''_w is the heat flux referred to the outer tube surface (W/m^2), α is the local heat transfer coefficient [W/(m^2·K)], and $T_{f,ref}$ is the selected local reference fluid temperature (°C or K). Equations (2) and (3) use the outer cylindrical area $2\pi r_w L$ and are valid under the same steady, one-dimensional assumptions as Equation (1).

The local bulk-fluid temperature and local absolute pressure were interpolated linearly between the inlet and outlet measurements:

$$T_{f,bulk}(z) = T_{f,in} + (T_{f,out} - T_{f,in})\, z/L \tag{4}$$

$$p_{abs}(z) = p_{atm} + p_{in,g} + (p_{out,g} - p_{in,g})\, z/L \tag{5}$$

where $T_{f,in}$ and $T_{f,out}$ are the measured inlet and outlet fluid temperatures (°C or K), p_{atm} is atmospheric pressure (Pa), and $p_{in,g}$ and $p_{out,g}$ are the measured inlet and outlet gauge pressures (Pa). Equations (4) and (5) assume linear axial variation between the inlet and outlet over $0 \leq z \leq L$.

The local saturation temperature was obtained from the water saturation relation, T_{sat}(z) = $T_{sat}[p_{abs}(z)]$ for water. In the present data set, $T_{f,bulk}$ was between 6.8 K and 125 K below T_{sat} at all analysed points. The complete series was therefore classified as bulk-subcooled, including later settings in which vapour bubbles were visually observed. Accordingly, $T_{f,ref} = T_{f,bulk}$ was used throughout the water analysis when calculating the local heat transfer coefficient.

The model does not distinguish a separate coating resistance. The calculated heat transfer coefficient should therefore be interpreted as an effective wall-fluid coefficient for the complete substrate–coating–fluid system under the stated assumptions.

5. Measurement Uncertainty and Comparison Protocol

5.1. Measurement Uncertainty

The present analysis is based on a comparative data-reduction procedure applied consistently to all smooth and modified surfaces. The principal measured quantities were electrical power, mass flow rate, inlet and outlet fluid temperatures, inlet and outlet pressures, and local thermocouple temperatures in the heated element. The accuracy of the measuring instruments is summarised in Table 3.

Table 3. Accuracy of the main measuring instruments used in the experimental setup.

Accuracy/Limiting Error	Measuring Instrument
±0.1% of measured value	Flow measurement (Coriolis mass flow metre)
±0.5 °C (nominal value adopted for uncertainty analysis)	Temperature measurement (Type T thermocouple)
±0.5% of span	Overpressure measurement (pressure transducers)
±1% of span	Atmospheric pressure measurement (pressure transmitter)
±(0.5% of reading + 0.6 V)	Power supply—output voltage
±(0.5% of reading + 0.02 A)	Power supply—output current
±(2% of reading + 1 W)	Power supply—output active power (displayed)
±(0.1% of reading + 0.5 °C)	Data acquisition (Type T thermocouple)
±0.1% of full scale	Data acquisition (voltage input)
±0.1% of voltage-range full scale; shunt resistor: ±0.005% of reading	Data acquisition (voltage input with 250 Ω shunt resistor)

Because the study focuses on pointwise differences between modified surfaces and the corresponding smooth references, the same geometrical assumptions and data-reduction equations were used for each compared pair. This approach limits the influence of systematic modelling assumptions on the relative ranking of the tested surfaces.

The uncertainty of the derived thermal quantities was evaluated using the law of propagation of uncertainty, following the procedure previously applied by Piasecka et al. [21]. The limiting errors specified for the individual components of the measurement chain were treated as Type-B contributions and converted to standard uncertainties assuming rectangular probability distributions. The combined standard uncertainty was obtained from the sensitivity-weighted input contributions, and expanded uncertainty was calculated using a coverage factor $k = 2$. The T-type thermocouples were additionally calibrated before the experimental campaign; however, the calibration-derived reduction in uncertainty was intentionally not used in the present budget. The nominal thermocouple accuracy and the nominal Graphtec GL840 Type-T input accuracy listed in Table 3 were therefore used.

The calculation was performed for a low-power operating point. The lowest heater-power setting in the steel + ZnO, 7 kg/h series was P = 110 W; for this setting, the axial position z = 0.01 m on the increasing-heat-flux branch had the smallest wall-to-bulk temperature difference among the ten thermocouple positions. The measured values were T_{TC} = 78.95 °C, $T_{f,in}$ = 42.10 °C, and $T_{f,out}$ = 51.25 °C. Using the same data-reduction model as in Section 4 gave T_w = 77.03 °C, $T_{f,bulk}$ = 42.93 °C, q''_w = 17.68 kW/m^2, and α = 519 W/(m^2·K). The corresponding expanded uncertainties were 3.70 W for heater power, 0.59 kW/m^2 for heat flux (3.36%), 0.89 K for T_w, 0.78 K for $T_{f,bulk}$, and 26 W/(m^2·K) for α, corresponding to 4.95%.

The uncertainty budget above represents instrumental/measurement uncertainty and does not absorb model-form assumptions such as the assumed thermocouple radius, substrate thermal conductivity, coating thermal resistance, axial conduction, or unmeasured external heat losses. These assumptions are treated separately in the model-sensitivity assessment. Pressure uncertainty was not propagated into α because $T_{f,bulk}$, rather than T_{sat}, was used as the reference temperature throughout the present water analysis; pressure remains relevant to the subcooling check. Run-to-run repeatability is likewise reported separately. In accordance with the calculated uncertainty level, absolute local and mean heat transfer coefficients are reported as whole numbers, whereas temperatures, temperature differences, and percentage changes in comparative summaries are reported to one decimal place.

5.2. Differential Comparison Protocol

Each modified surface was compared with one designated complete smooth-reference series having the same substrate and nominal mass flow rate. For copper, earlier smooth runs were retained only for independent repeatability assessment. This procedure avoids averaging multiple reference runs with markedly different baselines into an artificial reference curve.

Pointwise pairs were formed at the same nominal heat-flux level (corresponding to the same programmed heater-power setting), the same occurrence on the increasing- or decreasing-heat-flux branch, and the same axial thermocouple position. For every pair, the local relative change in the heat transfer coefficient and the wall-temperature difference were calculated. The pointwise relative change was defined as the percentage difference between the modified-surface value and the corresponding smooth-reference value, using the smooth-surface value as the reference denominator. Both the mean and median of the local relative changes were retained; the median was used as a robustness indicator because local ratios can be sensitive to small temperature differences.

For this study, a modification was classified as favourable only when the heat transfer coefficient increased, and the wall temperature decreased, or at least did not increase. The rule is a study-specific assessment criterion rather than a universal literature-derived threshold. Its purpose is to avoid classifying a surface as beneficial when a higher calculated coefficient is accompanied by a greater thermal demand at the wall. This coupled interpretation is consistent with the broader boiling literature, in which wettability, nucleation, rewetting and thermal performance must be considered jointly [1,6–8]. The increasing- and decreasing-heat-flux branches were preserved in the matching procedure, and each steady-state operating point was treated as a separate experimental state.

5.3. Model-Sensitivity Assessment

The propagated measurement uncertainty in Section 5.1 does not include model-form assumptions. A separate sensitivity assessment was therefore performed while retaining the experimental data and the comparative procedure. The purpose was not to replace the reported experimental results, but to quantify whether plausible changes in the principal modelling assumptions could alter their interpretation.

The conductivity values assumed in the calculations were compared with reference data for the corresponding material grades. For AISI 304/EN 1.4301 stainless steel, manufacturer data give approximately 14 W/(m·K) at 20 °C and 15 W/(m·K) at 100 °C [22], whereas a representative value of 339 W/(m·K) is reported for Cu-DHP/CW024A copper [23]. Replacing the assumed conductivity values with these reference values changed the reconstructed heat transfer coefficient by no more than approximately 0.7% for steel and 0.1% for copper. The sensitivity to the effective thermocouple coordinate was evaluated separately by varying it from 7.5 to 6.75 mm. The corresponding maximum change in the heat transfer coefficient was approximately 4.9% for steel and less than 0.3% for copper. This variation was used solely to assess model sensitivity and does not represent the physical conduction path from the thermocouple junction.

To assess sensitivity to the coating thermal properties, the coating was represented by its area-specific thermal resistance, R''_c, which was varied up to 3×10^{-5} m^2·K/W. Across this range, the maximum change in the reconstructed heat transfer coefficient was approximately 2.3%. The heater-tube contact resistance was evaluated parametrically in the same manner. A value of $R''_{cont} = 1 \times 10^{-5}$ $m^2 \cdot K/W$ corresponded to a typical wall-temperature correction of approximately 0.37 K. The resulting change in the heat transfer coefficient was generally below 1%, with a maximum of approximately 1.1% across the analysed data points.

Because the outer-glass temperature was unavailable, heat-loss sensitivity was evaluated by reducing the heat input used in the calculations by 2.5%, 5%, and 10%. Even at the 10% bound, the calculated heat transfer coefficient changed by approximately 10–11%, without altering the qualitative conclusions for any tested surface. Potential axial-conduction effects were considered separately. Because successive wall-temperature thermocouples were offset circumferentially by 36°, direct calculation of the axial second derivative would combine axial and circumferential temperature variations and amplify measurement scatter. A numerical axial-conduction correction was therefore not applied. Axial conduction remains a limitation of the one-dimensional model, particularly for copper.

Across all model-sensitivity ranges evaluated, the qualitative ranking of the tested surfaces remained unchanged. The ZnO coating on stainless steel remained the only modification showing a favourable combined response in terms of heat transfer coefficient and wall temperature at both nominal mass flow rates. Because model sensitivity concerns the assumptions used in the data reduction rather than measurement errors, it is reported separately from the propagated instrumental uncertainty. The reported heat transfer coefficients should therefore be interpreted as effective quantities representing the combined response of the substrate–coating–fluid system.

6. Results

6.1. Surface Descriptors: Contact Angle, Roughness and SEM Morphology

Figure 4 presents the water contact angles measured on samples with different coatings. Initially, the contact angles of the uncoated control samples were 105° for stainless steel (Figure 4a) and 90° for copper (Figure 4b). For the stainless-steel sample coated with Al_2O_3, the contact angle remained unchanged at 70° before (Figure 4(c1)) and after (Figure 4(c2)) the experiment. A similar result was observed for the copper sample coated with Al_2O_3, where the contact angle changed only slightly from 73° before (Figure 4(d1)) the experiment to 76° after (Figure 4(d2)) the experiment.

As shown in Figure 4, the stainless-steel sample coated with ZnO exhibited a contact angle of 98° (Figure 4(e1)) before the experiment and 115° (Figure 4(e2)) after the experiment. For the copper sample coated with ZnO, the corresponding values were 117° (Figure 4(f1)) and 119° (Figure 4(f2)). The stainless-steel sample coated with ZnO/PMHS exhibited contact angles of 145° (Figure 4(g1)) before and 140° (Figure 4(g2)) after the experiment, whereas the copper sample coated with ZnO/PMHS showed a decrease from 132° (Figure 4(h1)) to 122° (Figure 4(h2)). These measurements indicate that the final wetting state of the surfaces should be described using the measured contact-angle values rather than only the nominal coating type.

Figure 5 shows scanning electron microscope images of the samples coated with Al_2O_3, ZnO and ZnO/PMHS before and after the experiments, together with surface roughness values R_a. The uncoated stainless-steel and copper samples had relatively smooth surfaces, with R_a = 253.11 nm (Figure 5a) and R_a = 178.39 nm (Figure 5b), respectively. After coating with Al_2O_3, an aluminium-oxide layer was visible on the surface. The stainless-steel Al_2O_3 sample exhibited R_a = 1143.63 nm (Figure 5(c1)) before the experiment and R_a = 773.02 nm (Figure 5(c2)) after the experiment, together with a non-uniform distribution of aluminium-oxide granules. The copper Al_2O_3 sample showed a smaller decrease in roughness, from

R_a = 417.50 nm (Figure 5(d1)) before the experiment to R_a = 369.64 nm (Figure 5(d2)) after the experiment.

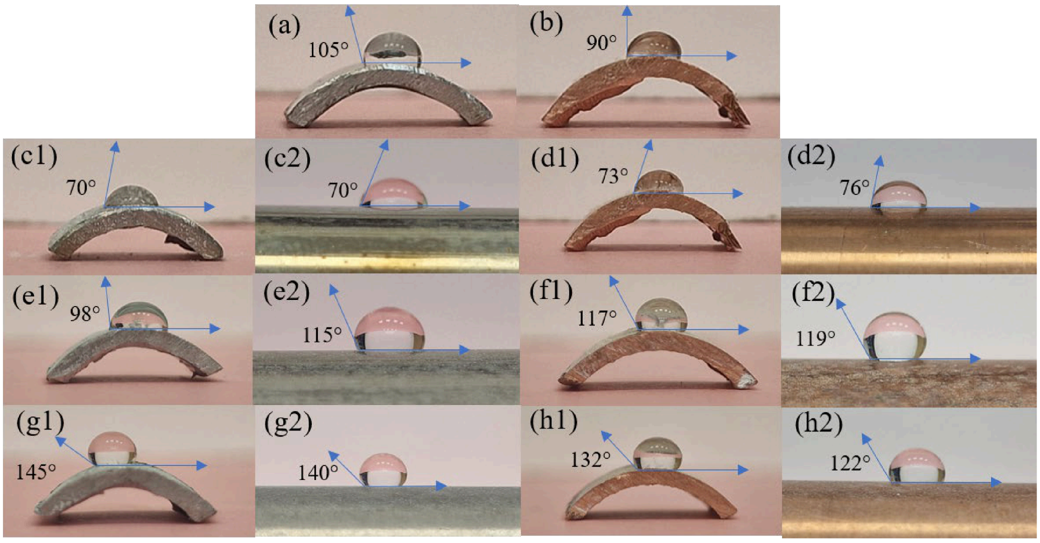

Figure 4. Water contact angles of the samples before the experiments: (**a**) steel, (**b**) copper, (**c1**) steel + Al_2O_3, (**d1**) copper + Al_2O_3, (**e1**) steel + ZnO, (**f1**) copper + ZnO, (**g1**) steel + ZnO/PMHS and (**h1**) copper + ZnO/PMHS; and after the experiments: (**c2**) steel + Al_2O_3, (**d2**) copper + Al_2O_3, (**e2**) steel + ZnO, (**f2**) copper + ZnO, (**g2**) steel + ZnO/PMHS and (**h2**) copper + ZnO/PMHS.

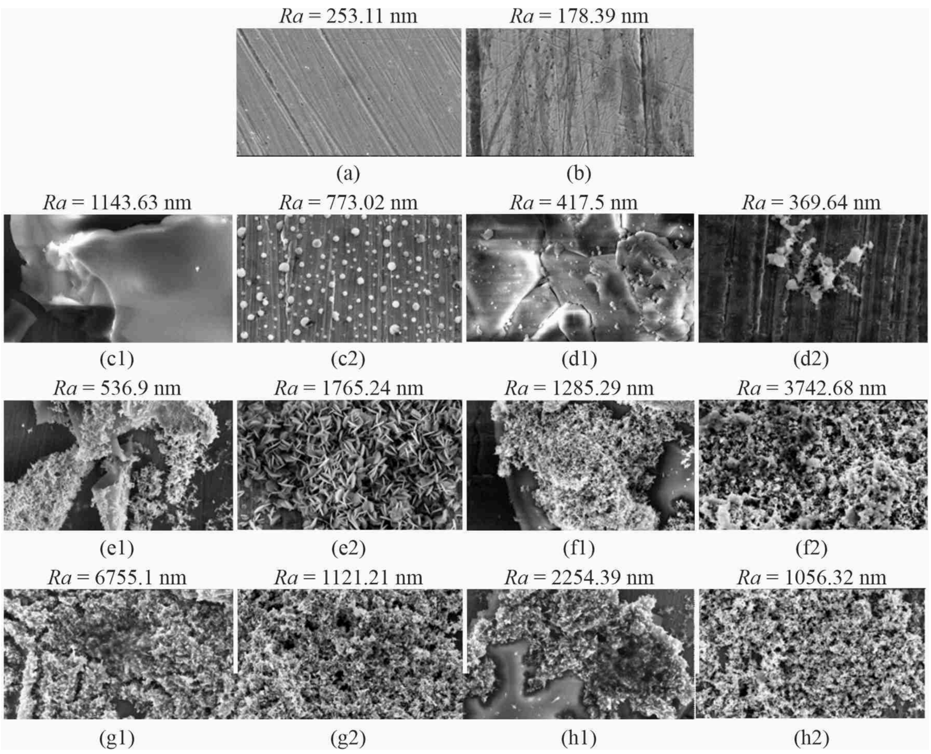

Figure 5. SEM images of the samples before the experiments with average roughness R_a: (**a**) steel, (**b**) copper, (**c1**) steel + Al_2O_3, (**d1**) copper + Al_2O_3, (**e1**) steel + ZnO, (**f1**) copper + ZnO, (**g1**) steel + ZnO/PMHS and (**h1**) copper + ZnO/PMHS; and after the experiments: (**c2**) steel + Al_2O_3, (**d2**) copper + Al_2O_3, (**e2**) steel + ZnO, (**f2**) copper + ZnO, (**g2**) steel + ZnO/PMHS and (**h2**) copper + ZnO/PMHS. All SEM images were acquired at a magnification of 5000×.

The ZnO-coated samples showed a marked increase in roughness after the experiments: from R_a = 536.9 nm (Figure 5(e1)) to R_a = 1765.24 nm (Figure 5(e2)) for stainless steel and from R_a = 1285.29 nm (Figure 5(f1)) to R_a = 3742.68 nm (Figure 5(f2)) for copper. In the SEM images, the ZnO tetrapod structures remained visible after exposure to water flow and temperature. A different roughness evolution was observed for ZnO/PMHS. The stainless-steel ZnO/PMHS sample decreased from R_a = 6755.10 nm (Figure 5(g1)) before the experiment to R_a = 1121.21 nm (Figure 5(g2)) after the experiment. The copper ZnO/PMHS sample decreased from R_a = 2254.39 nm (Figure 5(h1)) to R_a = 1056.32 nm (Figure 5(h2)). The images show fine ZnO tetrapods covered by a PMHS layer and a post-test surface morphology that is visibly smoother than before the experiment.

The surface descriptors extracted from the available contact-angle and roughness results are summarised in Table 4.

Table 4. Surface descriptors extracted from the available contact-angle and roughness results.

Comment	R_a After, nm	R_a Before, nm	Contact Angle After, °	Contact Angle Before, °	Tested	Specimen
Uncoated reference	—	253.11	—	105	Yes	Steel
Uncoated reference	—	178.39	—	90	Yes	Copper
Al_2O_3 coating tested thermally on steel	773.02	1143.63	70	70	Yes	Steel + Al_2O_3
Surface-characterisation specimen only	369.64	417.50	76	73	No	Copper + Al_2O_3
ZnO specimen; measured contact angle above 90°	1765.24	536.9	115	98	Yes	Steel + ZnO
ZnO specimen; measured contact angle above 90°	3742.68	1285.29	119	117	Yes	Copper + ZnO
Hydrophobic ZnO/PMHS specimen	1121.21	6755.10	140	145	Yes	Steel + ZnO/PMHS
Hydrophobic ZnO/PMHS specimen	1056.32	2254.39	122	132	Yes	Copper + ZnO/PMHS

6.2. General Thermal Response

The corrected bulk-subcooled analysis produced a clear separation between one favourable modification and the remaining surfaces. Figure 6 presents representative axial distributions of the local heat transfer coefficient for the steel surfaces at 290 W on the increasing-heat-flux branch, separately for nominal mass flow rates of 7 kg/h (Figure 6a) and 10 kg/h (Figure 6b). This figure shows how the local coefficient changes along the heated length and allows direct comparison between the smooth steel reference and the ZnO-, ZnO/PMHS- and Al_2O_3-modified steel surfaces under the same selected operating condition.

Figures 7 and 8 summarise the matched pointwise comparison for all tested modified surfaces. For each matched pair, the relative change in the local heat transfer coefficient was defined as the percentage difference between the modified-surface value and the corresponding smooth-reference value, normalised by the smooth-reference value. Figure 7 shows the mean and median relative changes in the local heat transfer coefficient with respect to the corresponding smooth reference of the same substrate and nominal mass flow rate. Figure 8 shows the corresponding mean wall-temperature change; negative values indicate that the modified surface operated at a lower wall temperature than the smooth reference. Taken together, Figures 7 and 8 allow the heat transfer coefficient response to be assessed together with the wall-temperature response, rather than treating coefficient enhancement alone as sufficient evidence of improvement. The corresponding numerical summary and thermal classification are provided in Table 5.

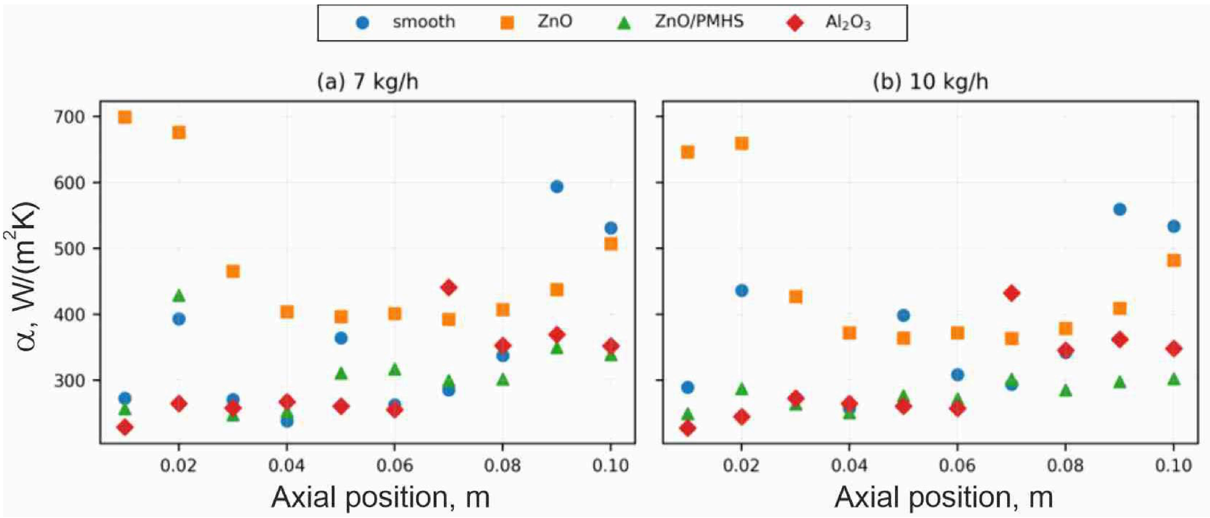

Figure 6. Local heat transfer coefficient along the steel tube for all tested steel surfaces at 290 W on the increasing-heat-flux branch: (**a**) 7 kg/h and (**b**) 10 kg/h.

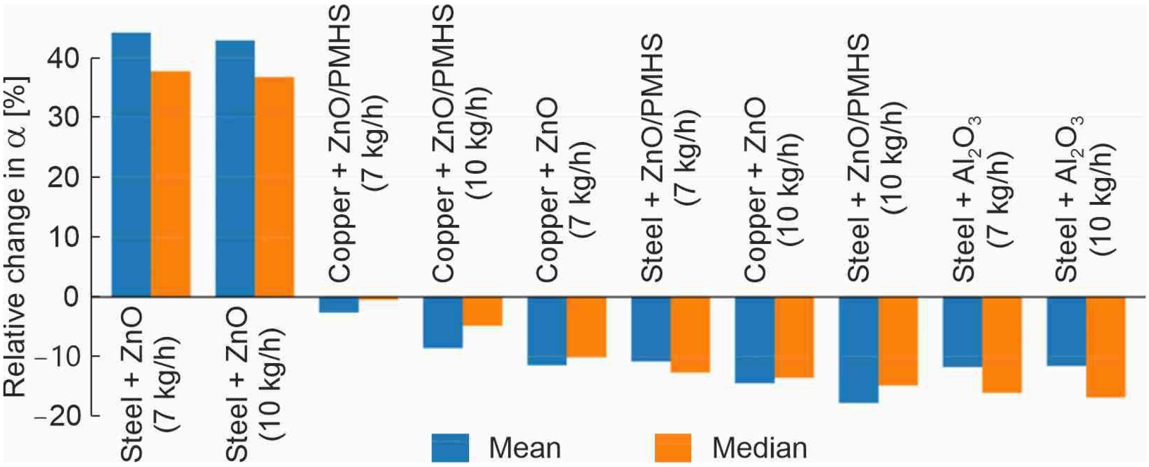

Figure 7. Mean and median pointwise relative changes in the local heat transfer coefficient with respect to the corresponding smooth reference.

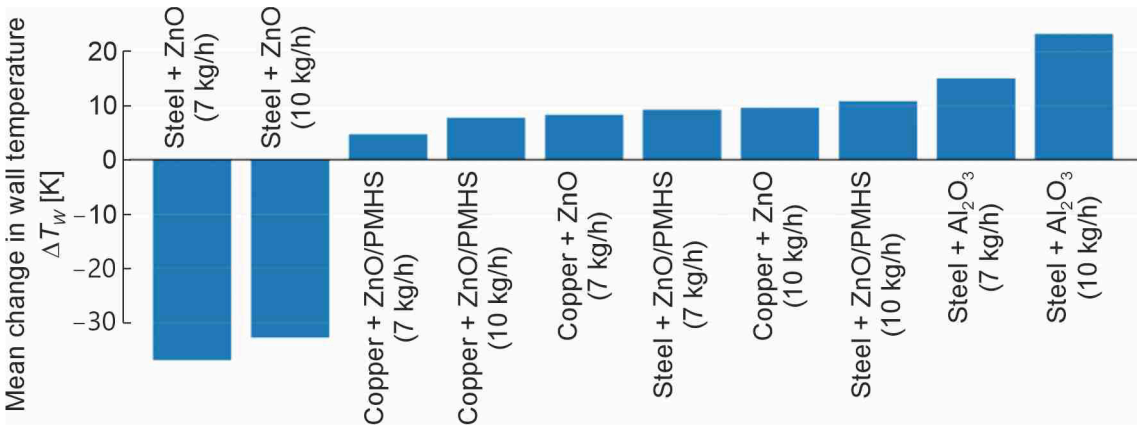

Figure 8. Mean wall-temperature change in each modified surface relative to the corresponding smooth reference. Negative values indicate a lower wall temperature.

Table 5. Bulk-subcooled differential performance of the modified surfaces relative to the corresponding smooth references.

Interpretation	Mean ΔT_w, K	Relative Change in α: Mean (Median), %	Mean α, W/(m^2·K)	Surface	Substrate and Flow Rate
Clear enhancement	−36.9	+44.2% (+37.8%)	439	ZnO	Steel, 7 kg/h
Clear enhancement	−32.8	+42.9% (+36.8%)	439	ZnO	Steel, 10 kg/h
Near-neutral α; no overall benefit	+4.7	−2.6% (−0.5%)	347	ZnO/PMHS	Copper, 7 kg/h
Unfavourable	+10.8	−11.4% (−10.1%)	310	ZnO	Copper, 7 kg/h
No enhancement	+8.3	−8.5% (−4.8%)	351	ZnO/PMHS	Copper, 10 kg/h
Unfavourable	+15.1	−14.4% (−13.5%)	314	ZnO	Copper, 10 kg/h
No enhancement	+7.8	−11.8% (−16.1%)	276	Al_2O_3	Steel, 7 kg/h
No enhancement	+9.6	−11.6% (−16.8%)	265	Al_2O_3	Steel, 10 kg/h
Unfavourable	+9.2	−10.7% (−12.7%)	274	ZnO/PMHS	Steel, 7 kg/h
Unfavourable	+23.3	−17.7% (−14.8%)	246	ZnO/PMHS	Steel, 10 kg/h

The detailed surface ranking is discussed in Sections 6.3–6.5. Because absolute local heat transfer coefficients varied substantially with axial position and experimental series, the interpretation is based primarily on matched differential results rather than on isolated local maxima.

6.3. Relative Heat Transfer Performance of Modified Surfaces

The differential comparison used all matched points from the bulk-subcooled formulation. For each modified surface, the corresponding smooth run was matched by nominal heat-flux level, increasing- or decreasing-heat-flux branch, and axial position. Table 5 reports the mean local heat transfer coefficient of the modified surface, the mean and median pointwise relative changes, and the mean wall-temperature difference. The same ranking is visualised in Figures 7 and 8.

The mean pointwise percentage change and the ratio of global means are not identical quantities. The former preserves the contribution of every matched local point, whereas the latter can be dominated by regions with larger absolute coefficients. The present ranking therefore reports the mean pointwise change together with its median.

When Table 5 is analysed together with Figures 7 and 8, steel + ZnO is the only surface that simultaneously increases the local heat transfer coefficient and lowers the wall temperature at both analysed flow rates. The mean pointwise enhancement exceeds 42%, while the corresponding medians are approximately 37%. The Al_2O_3 coating does not reproduce this effect: the coefficient decreases by about 12% on average, and the wall temperature increases by 7.8–9.6 K. The ZnO/PMHS steel coating also performs unfavourably, especially at 10 kg/h.

6.4. Steel Surfaces

The steel substrate showed the clearest coating-dependent response. In Figure 6, the ZnO-modified steel surface exhibits higher local coefficients over most of the heated length at both nominal mass flow rates. The aggregate comparison in Table 5 and Figures 7 and 8 confirms this trend: the mean local heat transfer coefficient was 439 W/(m^2·K) at 7 kg/h and 439 W/(m^2·K) at 10 kg/h, while the corresponding mean pointwise gains relative to smooth steel were 44.2% and 42.9%, with medians of 37.8% and 36.8%. Mean wall temperature decreased by 36.9 K and 32.8 K, respectively.

Neither ZnO/PMHS nor Al_2O_3 improved the steel reference. ZnO/PMHS reduced the mean local coefficient by 10.7% at 7 kg/h and 17.7% at 10 kg/h, while increasing wall temperature by 9.2 K and 23.3 K. Al_2O_3 reduced the mean local coefficient by approximately 11.6–11.8% and increased wall temperature by approximately 7.8–9.6 K. Thus, the favourable steel response was specific to ZnO rather than to oxide modification in general.

6.5. Copper Surfaces and Reference Repeatability

The copper modifications did not provide a robust benefit relative to the designated smooth references. Copper + ZnO reduced the mean local coefficient by 11.4% at 7 kg/h and 14.4% at 10 kg/h, while increasing mean wall temperature by 10.8 K and 15.1 K. Copper + ZnO/PMHS was closer to neutral at 7 kg/h, with a mean pointwise change of −2.6% and a median of −0.5%, but wall temperature still increased by 4.7 K. At 10 kg/h, copper + ZnO/PMHS reduced the mean local coefficient by 8.5% and increased wall temperature by 8.3 K.

The repeatability of the independent smooth copper reference runs is illustrated in Figure 9 by local heat transfer coefficient profiles as a function of axial position at a heater power of 290 W and at two nominal mass flow rates. The run-to-run discrepancies shown in Figure 9 are comparable to or greater than the apparent effects of the copper coatings. Therefore, none of the copper coatings can currently be classified as heat transfer enhancing. These conclusions apply only to the present distilled-water experiments and the selected smooth-reference runs. The response may differ in the planned experiments using refrigerants as working fluids, because their viscosity, surface tension, latent heat, saturation pressure and wetting behaviour differ substantially from those of water.

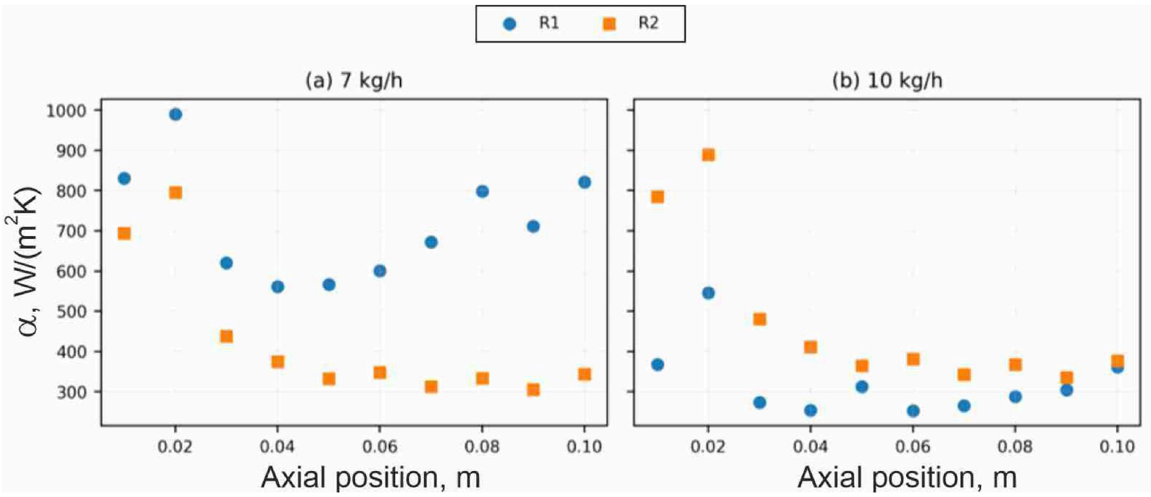

Figure 9. Repeatability of independent smooth copper reference runs illustrated by local heat transfer coefficient profiles at 290 W on the increasing-heat-flux branch: (**a**) 7 kg/h and (**b**) 10 kg/h. R1 and R2 denote separate experimental runs.

7. Discussion

The present results show that the thermal response of a modified surface in this annular minichannel cannot be inferred from coating chemistry, roughness, or static wettability considered separately. ZnO on stainless steel was the only modification that satisfied both thermal assessment criteria at both nominal mass flow rates, whereas the other steel coatings and both copper modifications did not show a favourable combined response. This surface-specific behaviour is consistent with the broader literature showing that modified or roughened surfaces do not automatically provide boiling enhancement [1,4,5].

The favourable behaviour of ZnO on stainless steel cannot be explained by a simple hydrophilic-versus-hydrophobic classification. The measured water contact angle of the steel + ZnO specimen was 98° before the experiment and 115° after it, while its roughness increased from R_a = 536.9 nm to 1765.24 nm. Thus, the surface producing the strongest thermal enhancement was not the most hydrophilic surface in the tested matrix. This observation agrees with literature showing that the boiling response of nanostructured surfaces is governed by a coupled interaction between wettability and morphology rather than by static contact angle alone. Phan et al. [7] demonstrated a strong influence of surface wettability on water flow boiling in a nanocoated microchannel, while the review by Mardosaitė et al. [9] shows that the wetting behaviour of ZnO nanostructures additionally depends on their morphology, surface defects and the possibility of Wenzel- or Cassie–Baxter-type wetting states. Consequently, the present enhancement should be interpreted as a response of the complete ZnO–steel–water interface rather than as a direct consequence of the measured contact angle.

The post-test surface characterisation provides an additional indication that morphology may be relevant. For steel + ZnO, the ZnO tetrapod structures remained visible after the experiments and the measured R_a increased substantially. Such a developed structure may provide geometrical features favourable for vapour embryo formation and bubble departure while maintaining pathways for liquid access to the heated wall. This interpretation is consistent with studies in which increased multiscale roughness and surface development promoted boiling, particularly through an increased availability of active nucleation sites [13]. However, the present experiments did not provide direct measurements of nucleation-site density, bubble departure diameter or local liquid-film behaviour. Therefore, the surface-characterisation results support a plausible mechanism but do not by themselves prove which microscopic process was responsible for the measured heat transfer-coefficient enhancement.

The unfavourable response of ZnO/PMHS on stainless steel is particularly informative because it demonstrates that increasing hydrophobicity does not necessarily improve flow boiling. The steel + ZnO/PMHS specimen had the highest initial contact angle among the steel surfaces, approximately 145°, but its mean local heat transfer coefficient decreased by 10.7% at 7 kg/h and by 17.7% at 10 kg/h, while the mean wall temperature increased by 9.2 K and 23.3 K, respectively. In parallel, its measured roughness decreased markedly after the experiment, from R_a = 6755.10 nm to 1121.21 nm. The thermal response was therefore opposite to that of ZnO on the same substrate.

One possible explanation is that the low-surface-energy modification changed the balance between vapour nucleation and liquid replenishment. Hydrophobic regions can facilitate vapour embryo formation, but excessive vapour retention or a reduction in effective liquid–solid contact may increase wall temperature. This general competition is consistent with the observations of Betz et al. [6], who found that neither uniformly superhydrophilic nor uniformly superhydrophobic surfaces necessarily provided the optimum boiling response, and with mixed-wettability microchannel studies showing the importance of balancing nucleation and liquid supply [8]. The ZnO tetrapod studies discussed in [18] likewise demonstrate that hydrophobic functionalisation can strongly alter vapour-layer behaviour, although the Leidenfrost-related conditions considered there differ substantially from the subcooled flow boiling conditions of the present experiments. Accordingly, the present data should not be interpreted as evidence that hydrophobic ZnO/PMHS is generally detrimental, but rather that this particular coating–substrate–fluid combination was unfavourable under the tested conditions.

The Al_2O_3 results provide a complementary example. Steel + Al_2O_3 had a substantially lower contact angle of approximately 70° and was therefore more wettable than either ZnO-modified steel surface. Nevertheless, its local heat transfer coefficient decreased by approximately 12% relative to smooth steel, and its mean wall temperature increased by approximately 8–10 K. Its roughness also decreased after testing, from R_a = 1143.63 nm to 773.02 nm. Thus, neither increased wettability nor the presence of a ceramic oxide was sufficient to produce enhancement. This result reinforces the central finding that nominal coating chemistry and static contact angle alone cannot be used as predictors of flow boiling performance. Previous investigations of oxide-coated surfaces have likewise shown strongly coating-dependent thermal and vapour-layer behaviour [17], although direct quantitative comparison is not appropriate because those experiments concerned Leidenfrost conditions rather than confined subcooled flow boiling.

The comparison between the two substrates further demonstrates that the coating material cannot be considered independently of the substrate. ZnO strongly enhanced heat transfer on stainless steel but did not provide a measurable benefit on copper. At the same time, the copper + ZnO specimen exhibited a comparable static contact angle to steel + ZnO and an even larger post-test roughness (R_a = 3742.68 nm). If contact angle or roughness alone controlled the thermal response, qualitatively similar enhancement would be expected for the two ZnO-coated substrates. This was not observed.

Several effects may contribute to this substrate dependence. Copper and stainless steel differ strongly in thermal conductivity, which changes radial and axial heat spreading within the heated tube. The substrate may also affect coating adhesion, local morphology, interfacial thermal resistance and the thermal conditions experienced by individual nucleation sites. Since the present heat transfer coefficient is an effective coefficient for the complete substrate–coating–fluid system and the coating thermal resistance was not resolved separately, the contributions of these mechanisms cannot be isolated from the available data. Nevertheless, the opposite ZnO responses on copper and steel support treating the coating–substrate combination, rather than coating identity alone, as the functional boiling surface.

The surface descriptors also show quantitatively that no simple monotonic relation with the thermal ranking can be inferred from the present matrix. After testing, steel + ZnO had a water contact angle of 115° and R_a = 1765 nm while producing mean pointwise coefficient increases of approximately 44% and 43% at the two flow rates. Copper + ZnO had a similar contact angle of 119° and a higher R_a of 3743 nm, yet its mean response was approximately −11% and −14%. Steel + ZnO/PMHS combined a 140° contact angle with R_a = 1121 nm and negative responses of approximately −11% and −18%, whereas steel + Al_2O_3 had a much lower 70° contact angle and also showed a negative response. With only a small number of non-independent surface configurations, a formal regression or significance claim would not be statistically defensible; the defensible conclusion is the observed absence of a one-parameter monotonic trend.

The strong axial variation in the local heat transfer coefficient observed in Figure 6 is also physically consistent with previous annular-minigap studies. Even though the complete present data set remained bulk-subcooled, the local fluid temperature increased downstream, and the degree of local subcooling consequently changed along the heated section. When vapour generation occurred, bubble population, nucleation activity, condensation and liquid replenishment could also evolve with axial position. Chen et al. [3] demonstrated experimentally that heat flux, inlet subcooling and annular gap size affect not only the boiling heat transfer coefficient but also bubble departure diameter, departure frequency and active nucleation-site density. Boye et al. [2] likewise showed that the effects of heat flux, mass flux and vapour quality in narrow annular gaps are coupled rather than independent.

Similar axial trends have been reported for HFE-649 boiling in annular minigaps. Hożejowska and Piasecka [19] obtained strongly varying local coefficients along a 2 mm annular minigap, with a general downstream decrease in the analysed saturated-boiling region. Experiments with several enhanced surfaces in a 1 mm minigap also showed that the local coefficient commonly decreased with distance from the inlet [4]. The separate study [5] considered flow resistance together with heat transfer in a different annular-minigap apparatus and is therefore not used here as a direct hydraulic comparator. The axial non-uniformity in the present experiments should not be treated as an experimental anomaly or as a coating effect alone. It is an inherent consequence of the developing thermal and boiling conditions in the annular channel, superimposed on the local influence of the tested surface.

To place the present result in the context of directly relevant flow boiling work, Table 6 summarises representative studies that address wettability-modified microchannels, annular gap boiling, enhanced surfaces, and, separately, flow-resistance assessment. The comparison emphasises that the present contribution is the matched thermal comparison of several coating–substrate combinations under the same annular-minichannel conditions.

Table 6. Comparison with selected directly relevant flow boiling and annular-minigap studies.

Main Relevance to the Present Study	Surface or Variable	Geometry/Fluid	Study
Demonstrated a strong influence of wettability on flow boiling heat transfer in a microchannel.	Nanocoated surfaces; wettability	Single rectangular microchannel/water	Phan et al. [7]
Reported up to 56.7% heat transfer enhancement on biphilic surfaces and linked the improvement to changes in bubbly and slug flow regimes.	Gradient mixed wettability	High-aspect-ratio microchannel/flow boiling	Ahmadi et al. [8]
Showed coupled effects of gap width, heat flux, mass flux, inlet temperature, and vapour quality.	Gap width and operating parameters	Annular gaps 0.5–1.5 mm/n-hexane	Boye et al. [2]
Linked heat transfer changes with bubble departure, frequency, and active nucleation-site density.	Gap, heat flux, subcooling, bubble characteristics	Annular ducts 1–2 mm/R-407C	Chen et al. [3]
Demonstrated that enhancement is surface-specific; one enhanced surface outperformed the smooth reference while another did not.	Mechanically/electrochemically enhanced copper surfaces	1 mm annular minigap/HFE-649	Piasecka et al. [4]
Separate study of heat transfer and flow resistance in a different annular-minigap module and measurement system; cited as complementary hydraulic work, not as a direct pressure-drop comparator for the present test section.	Smooth vs threaded surface; pressure-drop modelling	2 mm annular minigap/HFE-649	Piasecka et al. [5]
Matched pointwise comparison shows a favourable response only for ZnO/steel within the tested matrix; coating identity alone does not predict performance.	ZnO, ZnO/PMHS, Al_2O_3 on steel/copper	1.2 mm annular minichannel/distilled water	Present study

In addition, because the local coefficient is calculated from the local temperature difference $T_w - T_{f,bulk}$, its relative sensitivity increases when this denominator becomes small. This provides an additional reason for avoiding interpretation based on isolated local maxima and supports the use of matched pointwise distributions, means and medians adopted in the present study.

The comparison of the two nominal mass flow rates provides a limited robustness check across operating conditions, but it is not a repeatability test. For steel + ZnO, the mean enhancement remained similar, changing from 44.2% at 7 kg/h to 42.9% at 10 kg/h, with similarly close medians. This agreement shows that the favourable differential response occurred at both tested flow rates, but two operating conditions cannot establish generality. The deterioration produced by steel + ZnO/PMHS became stronger at the higher flow rate. Previous annular gap studies show that mass flux interacts with heat flux, gap size, subcooling, and local two-phase state [2,3]; the present ranking therefore should not be extrapolated beyond the tested range.

The copper results require a different level of confidence because the independent smooth-reference series show substantial run-to-run variability. At the selected condition illustrated in Figure 9, the differences between the smooth copper runs are comparable to or larger than the apparent effect of the ZnO and ZnO/PMHS modifications. Consequently, the available data do not support classification of either copper coating as heat transfer enhancing. This does not demonstrate that the coatings are intrinsically ineffective on copper; it means that their apparent effects cannot be separated robustly from the observed baseline variability within the present experimental data set.

This observation also explains why the use of one designated complete smooth-reference series and matched pointwise comparisons is preferable to constructing an averaged reference from mutually inconsistent runs. The agreement between the mean and median responses for steel + ZnO provides additional support for its ranking, whereas the near-zero median for copper + ZnO/PMHS at 7 kg/h confirms the absence of a robust enhancement despite individual local differences.

Finally, the interpretation of the present coating effects should remain within the resolution of the experimental methodology. Static contact angle and R_a provide useful but incomplete descriptors of the functional boiling surface; they do not quantify contact-angle hysteresis, spatial heterogeneity of the coating or the dynamic wetting state during boiling. The interpretation of static contact-angle values also requires caution because the measured value depends on the measurement procedure and profile-fitting method [10]. Similarly, the present effective heat transfer coefficient includes the combined response of the substrate, coating and fluid because the individual coating thermal resistance was not separated. The before/after SEM and roughness measurements demonstrate that the surfaces changed differently during testing, but they do not establish the time at which those changes occurred. These limitations do not alter the comparative ranking obtained under identical data-reduction assumptions, but they prevent attribution of the observed enhancement to a single microscopic mechanism. The most defensible conclusion is therefore that, among the tested configurations, the ZnO–stainless-steel combination provided a consistent thermal advantage under the tested conditions, whereas neither oxide chemistry, high roughness nor high static contact angle alone predicted the observed performance.

Scope and Limitations of the Present Comparison

Independent replicate runs were not available for every modified surface, and matched axial points are therefore treated as local observations within individual experimental series rather than as independent experiments. The smooth copper repeat runs characterise baseline variability only for that reference case. Accordingly, the ZnO/steel result is interpreted as a consistent differential response within the investigated matrix, not as independently replicated evidence of general coating superiority. Accordingly, no inferential statistical significance is claimed for differences between coating types, and the terms "best-performing" and "most promising" refer only to the present tested matrix and operating conditions.

The data reduction uses a simplified one-dimensional radial-conduction model with an effective thermocouple coordinate. Section 5.3 evaluates sensitivity to substrate conductivity, the effective coordinate, coating and contact resistance, and bounded heat loss; none of these variations changed the qualitative surface ranking. Axial conduction was not corrected numerically because the circumferentially staggered thermocouples do not provide a purely axial temperature curvature. The reported heat transfer coefficient is therefore interpreted as an effective response of the substrate–coating–fluid system.

The present study addresses thermal performance. Pressure measurements were used to determine local absolute pressure and saturation temperature, not to rank surfaces by pressure drop. Flow resistance was investigated separately in [5] using a different experimental module and measurement system; therefore, no direct quantitative comparison is made. The favourable thermal response of ZnO/steel should not be interpreted as evidence of thermo-hydraulic optimality.

The conclusions are limited to distilled water, two nominal mass flow rates, the 1.2 mm annular gap, and the investigated heat-flux sequence. Extension to other fluids and operating ranges requires broader independently replicated data and matched thermal and hydraulic measurements. The harmonised database and leakage-safe workflow reported in [24] provide a basis for future data-driven assessment of coupled surface descriptors and development of improved heat transfer correlations.

8. Conclusions

Subcooled flow boiling of distilled water was investigated in a 1.2 mm annular minichannel using smooth and ZnO-, ZnO/PMHS-, and Al_2O_3-modified heated tubes on copper and stainless-steel substrates. The analysis used a simplified cylindrical wall-temperature correction and matched pointwise comparison with a designated smooth reference of the same substrate and nominal mass flow rate.

All analysed local bulk temperatures remained below the corresponding local saturation temperatures by at least 6.8 K; the data set was therefore treated as bulk-subcooled, including settings at which vapour bubbles were visually observed.

Within the tested matrix, ZnO-modified stainless steel produced the strongest favourable thermal response. The mean pointwise heat transfer coefficient increased by 44.2% at 7 kg/h and 42.9% at 10 kg/h, with medians of 37.8% and 36.8%, while the mean wall temperature decreased by 36.9 K and 32.8 K. Similar responses at the two flow rates show consistency across those two operating conditions but do not constitute independent repeatability or justify extrapolation beyond the tested range.

Al_2O_3 and ZnO/PMHS on stainless steel did not provide a favourable combined response, and neither copper modification showed a robust improvement relative to its designated smooth reference. The opposite response of nominally similar ZnO coatings on steel and copper indicates that coating identity, static contact angle, or roughness alone cannot explain the observed ranking; the coating–substrate–fluid system must be considered as a coupled thermal interface.

The engineering conclusion is therefore deliberately limited: ZnO/steel is the most promising configuration among those tested here, not a universally superior boiling surface. A separate model-sensitivity assessment showed that the bounded variations considered for substrate conductivity, effective thermocouple radius, coating resistance, heater-tube contact resistance, and external heat loss did not alter the qualitative surface ranking. Nevertheless, the absolute coefficients remain subject to the simplified one-dimensional model, axial conduction was not resolved independently, coating properties were not measured specimen-by-specimen, and independent repeats were not available for all modified surfaces. The present paper is restricted to thermal performance; flow resistance is outside its scope and has been considered separately in [5] for a different annular-minigap module and measurement system. Additional fluids, operating ranges, replicate runs, direct coating/contact characterisation, outer-glass heat-loss measurements, and dedicated hydraulic measurements are required before broader design recommendations can be made.

From an application perspective, these findings may support the preliminary selection of surface–substrate combinations for compact two-phase cooling systems, flow boiling evaporators, and high-heat-flux thermal-management devices operating under bulk-subcooled conditions. At the present stage, however, the results should be treated as preliminary comparative evidence rather than as a design correlation or a direct recommendation for industrial implementation. Practical application of the ZnO/steel configuration will require verification of coating durability, manufacturability, fouling resistance, long-term stability, hydraulic penalty, and performance under device-specific thermal and flow conditions. The next stage of the research should therefore combine replicate experiments over extended operating ranges with direct characterisation of coating and contact properties, improved conjugate heat transfer and heat-loss modelling, and simultaneous thermal–hydraulic assessment in geometries representative of the intended applications. Once a broader, independently replicated database becomes available, it could also support the development and external validation of predictive heat transfer correlations and machine-learning models accounting for the coupled effects of substrate, coating, flow conditions, and thermal boundary conditions.

Author Contributions: Conceptualization, M.P.; methodology, M.P. and S.R.; software, M.P.; validation, M.P. and K.G.; formal analysis, M.P., K.G., and A.P.; investigation, K.G. and M.M.; resources, M.P., and R.S.; data curation, M.P.; writing—original draft preparation, M.P., A.P., R.S., and A.A.; writing—review and editing, M.P., A.P., M.M., and R.S.; visualisation, A.P. and A.A.; supervision, M.P.; project administration, M.P.; funding acquisition, M.P. and R.S. All authors have read and agreed to the published version of the manuscript.

Funding: This research was funded by the National Science Centre, Poland, grant no. UMO-2025/57/B/ST8/00907.

Data Availability Statement: The experimental data supporting the findings of this study, together with the associated metadata and calculation files, are archived in the PRACE-LAB data-storage infrastructure at Kielce University of Technology and are available from the corresponding author upon reasonable request. The data are not publicly available due to ongoing related research and preparation of follow-up analyses.

Acknowledgments: Simas Račkauskas acknowledges financial support from the Research Council of Lithuania (LMTLT) and the Ministry of Education, Science and Sport of the Republic of Lithuania under agreement No. S-A-UEI-23-1 for the preparation of the ZnO materials and modified surfaces investigated in this work.

Conflicts of Interest: The authors declare no conflicts of interest.

Nomenclature

Symbol	Description	Unit
k	Coverage factor	-
k_s	Thermal conductivity of the substrate material	W/(m·K)
L	Active heated length of the test section	m
P	Electrical heater power used in the data-reduction model	W
p_{abs}	Local absolute pressure in the minichannel	Pa

p_{atm}	Atmospheric pressure	Pa
$p_{in,g}$	Gauge pressure measured at the test-section inlet	Pa
$p_{out,g}$	Gauge pressure measured at the test-section outlet	Pa
q''_w	Heat flux referred to the outer surface of the heated metal tube	W/m^2
R_a	Arithmetic mean surface roughness	nm or µm
R''_c	Area-specific thermal resistance of the coating used in the model-sensitivity assessment	$m^2 \cdot K/W$
R''_{cont}	Area-specific heater-tube contact resistance used parametrically in the model-sensitivity assessment	$m^2 \cdot K/W$
r_{TC}	Assumed radial position of the thermocouple temperature in the simplified model	m
r_w	Outer radius of the heated metal tube; wall–fluid interface radius	m
$T_{f,bulk}$	Local bulk-fluid temperature	°C or K
$T_{f,in}$	Fluid temperature measured at the test-section inlet	°C or K
$T_{f,out}$	Fluid temperature measured at the test-section outlet	°C or K
$T_{f,ref}$	Reference fluid temperature used in the heat transfer-coefficient definition	°C or K
T_{sat}	Local saturation temperature calculated from local absolute pressure	°C or K
T_{TC}	Thermocouple temperature measured in the heated element	°C or K
T_w	Calculated local wall temperature at the heated-tube–fluid interface	°C or K
z	Axial coordinate measured from the test-section inlet	m
Greek symbols		
α	Local heat transfer coefficient at the wall–fluid interface	$W/(m^2 \cdot K)$
$\Delta\alpha/\alpha_{ref}$	Pointwise relative change in local heat transfer coefficient with respect to the corresponding smooth reference	%
ΔT_w	Pointwise or mean wall-temperature change relative to the corresponding smooth reference	K
Abbreviations and coating names		
Al_2O_3	Aluminium oxide	-
PMHS	Polymethylhydrosiloxane	-
SEM	Scanning electron microscopy	-
TEOS	Tetraethyl orthosilicate	-
ZnO	Zinc oxide	-
ZnO/PMHS	ZnO coating modified with PMHS	-

References

1. Liang, G.; Mudawar, I. Review of channel flow boiling enhancement by surface modification, and instability suppression schemes. *Int. J. Heat. Mass. Transf.* **2020**, *146*, 118864. [CrossRef]
2. Boye, G.; Schmidt, J.; Beyrau, F. Analysis of flow boiling heat transfer in narrow annular gaps applying the design of experiments method. *Adv. Mech. Eng.* **2015**, *7*, 1–14. [CrossRef]
3. Chen, C.A.; Chang, W.R.; Li, K.W.; Lie, Y.M.; Lin, T.F. Subcooled flow boiling heat transfer of R-407C and associated bubble characteristics in a narrow annular duct. *Int. J. Heat. Mass. Transf.* **2009**, *52*, 3147–3158. [CrossRef]
4. Piasecka, M.; Musiał, T.; Piasecki, A. Cooling liquid flow boiling heat transfer in an annular minigap with an enhanced wall. *EPJ Web Conf.* **2019**, *213*, 02066. [CrossRef]
5. Piasecka, M.; Hożejowska, S.; Wolak, W. Flow Resistance and Heat Transfer During Flow Boiling of HFE-649 in an Annular Minigap. *Energies* **2026**, *19*, 2689. [CrossRef]
6. Betz, A.R.; Jenkins, J.; Kim, C.-J.; Attinger, D. Boiling heat transfer on superhydrophilic, superhydrophobic, and superbiphilic surfaces. *Int. J. Heat. Mass. Transf.* **2013**, *57*, 733–741. [CrossRef]
7. Phan, H.T.; Caney, N.; Marty, P.; Colasson, S.; Gavillet, J. Flow boiling of water on nanocoated surfaces in a microchannel. *J. Heat. Transf.* **2012**, *134*, 020901. [CrossRef]
8. Ahmadi, V.E.; Aboubakri, A.; Khalili Sadaghiani, A.; Sefiane, K.; Koşar, A. Effect of functional surfaces with gradient mixed wettability on flow boiling in a high aspect ratio microchannel. *Fluids* **2020**, *5*, 239. [CrossRef]
9. Mardosaitė, R.; Jurkevičiūtė, A.; Račkauskas, S. Superhydrophobic ZnO nanowires: Wettability mechanisms and functional applications. *Cryst. Growth Des.* **2021**, *21*, 4765–4779. [CrossRef]
10. Wciślik, S.; Kotrys-Działak, D.; Taler, D. Influence of dosing parameters and droplet profile fitting methods on static contact angle determination in TiO_2 nanofluids. *Int. J. Heat. Mass. Transf.* **2026**, *269*, 129169. [CrossRef]
11. Kaniowski, R.; Wciślik, S. Thermal Performance Enhancement in Pool Boiling on Copper Surfaces: Contact Angle and Surface Tension Analysis. *Energies* **2025**, *18*, 4471. [CrossRef]

12. Radek, N.; Konstanty, J.; Pietraszek, J.; Orman, Ł.J.; Szczepaniak, M.; Przestacki, D. The Effect of Laser Beam Processing on the Properties of WC-Co Coatings Deposited on Steel. *Materials* **2021**, *14*, 538. [CrossRef]
13. Orman, Ł.J.; Radek, N.; Pietraszek, J.; Wojtkowiak, J.; Szczepaniak, M. Laser Treatment of Surfaces for Pool Boiling Heat Transfer Enhancement. *Materials* **2023**, *16*, 1365. [CrossRef]
14. Żórawski, W.; Chatys, R.; Radek, N.; Borowiecka-Jamrozek, J. Plasma-sprayed composite coatings with reduced friction coefficient. *Surf. Coat. Technol.* **2008**, *202*, 4578–4582. [CrossRef]
15. Lu, G.; Wang, J. Experimental investigation on heat transfer characteristics of water flow in a narrow annulus. *Appl. Therm. Eng.* **2008**, *28*, 8–13. [CrossRef]
16. Yang, Y.; Yuan, X.; Li, Z. Experimental and numerical study on heat transfer performance of single-phase water in a horizontal mini-annular channel. *Int. J. Heat. Fluid. Flow.* **2024**, *108*, 109483. [CrossRef]
17. Maziukienė, M.; Striūgas, N.; Vorotinskienė, L.; Skvorčinskienė, R.; Urbonavičius, M. The identification of Leidenfrost phenomenon formation on TiO_2-coated surfaces and the modelling of heat transfer processes. *Materials* **2024**, *17*, 3687. [CrossRef]
18. Vorotinskienė, L.; Antanavičė, A.; Skvorčinskienė, R.; Račkauskas, S.; Urbonavičius, M.; Kriūkienė, R.; Maziukienė, M. Effect of hydrophobicity of ZnO tetrapods coating on vapour film formation and friction reduction: A study using complex approach. *Int. J. Therm. Sci.* **2026**, *220*, 110372. [CrossRef]
19. Hożejowska, S.; Piasecka, M. Numerical solution of axisymmetric inverse heat conduction problem by the Trefftz method. *Energies* **2020**, *13*, 705. [CrossRef]
20. Tamulevičius, T.; Laurikėnas, P.; Juodėnas, M.; Mardosaitė, R.; Abakevičienė, B.; Pereyra, C.J.; Račkauskas, S. Antireflection Coatings Based on Randomly Oriented ZnO Nanowires. *Sol. RRL* **2023**, *7*, 2201056. [CrossRef]
21. Piasecka, M.; Maciejewska, B.; Michalski, D.; Dadas, N.; Piasecki, A. Investigations of Flow Boiling in Mini-Channels: Heat Transfer Calculations with Temperature Uncertainty Analyses. *Energies* **2024**, *17*, 791. [CrossRef]
22. Alleima. Sanmac 304/304L: Material Datasheet; Thermal Conductivity 14 W/(m·K) at 20 °C and 15 W/(m·K) at 100 °C. Available online: https://www.alleima.com/en/technical-center/material-datasheets/billets/sanmac-304304l/ (accessed on 17 August 2026).
23. Aurubis Finland Oy. Cold Rolled Plates: Pure Copper Alloys and Low-Alloyed Copper; Cu-DHP (CW024A) Thermal Conductivity 339 W/(m·K). Available online: https://www.aurubis.com/en/finland/industrial-products/cold-rolled-plates (accessed on 17 August 2026).
24. Piasecka, M.; Piasecki, A. A Unified Experimental Database, Data Harmonisation Workflow and Leakage-Safe Pilot Machine Learning for Flow Boiling in Rectangular Minichannels. *Preprints* **2026**. [CrossRef]